AGU PUBLICATIONS

JGR

Journal of Geophysical Research: Atmospheres

RESEARCH ARTICLE
10.1002/2015JD024603

Key Points:
- Dynamical response to two eruption strengths is simulated with an Earth system model
- Changes in wave propagation lead to strengthened polar vortex
- Ensemble spread is reduced under very strong volcanic forcing

Supporting Information:
- Supporting Information S1

Correspondence to:
M. Bittner,
matthias.bittner@mpimet.mpg.de

Citation:
Bittner, M., C. Timmreck, H. Schmidt, M. Toohey, and K. Krüger (2016), The impact of wave-mean flow interaction on the Northern Hemisphere polar vortex after tropical volcanic eruptions, *J. Geophys. Res. Atmos.*, *121*, doi:10.1002/2015JD024603.

Received 3 DEC 2015
Accepted 13 APR 2016
Accepted article online 28 APR 2016

The impact of wave-mean flow interaction on the Northern Hemisphere polar vortex after tropical volcanic eruptions

Matthias Bittner[1,2], Claudia Timmreck[1], Hauke Schmidt[1], Matthew Toohey[3], and Kirstin Krüger[4]

[1]Max Planck Institute for Meteorology, Hamburg, Germany, [2]International Max Planck Research School on Earth System Modelling (IMPRS), Hamburg, Germany, [3]GEOMAR, Helmholtz Centre for Ocean Research Kiel, Kiel, Germany, [4]Department of Geosciences, University of Oslo, Oslo, Norway

Abstract The current generation of Earth system models that participate in the Coupled Model Intercomparison Project phase 5 (CMIP5) does not, on average, produce a strengthened Northern Hemisphere (NH) polar vortex after large tropical volcanic eruptions as suggested by observational records. Here we investigate the impact of volcanic eruptions on the NH winter stratosphere with an ensemble of 20 model simulations of the Max Planck Institute Earth system model. We compare the dynamical impact in simulations of the very large 1815 Tambora eruption with the averaged dynamical response to the two largest eruptions of the CMIP5 historical simulations (the 1883 Krakatau and the 1991 Pinatubo eruptions). We find that for both the Tambora and the averaged Krakatau-Pinatubo eruptions the radiative perturbation only weakly affects the polar vortex directly. The position of the maximum temperature anomaly gradient is located at approximately 30°N, where we obtain significant westerly zonal wind anomalies between 10 hPa and 30 hPa. Under the very strong forcing of the Tambora eruption, the NH polar vortex is significantly strengthened because the subtropical westerly wind anomalies are sufficiently strong to robustly alter the propagation of planetary waves. The average response to the eruptions of Krakatau and Pinatubo reveals a slight strengthening of the polar vortex, but individual ensemble members differ substantially, indicating that internal variability plays a dominant role. For the Tambora eruption the ensemble variability of the zonal mean temperature and zonal wind anomalies during midwinter and late winter is significantly reduced compared to the volcanically unperturbed period.

1. Introduction

Satellite and radiosonde observations of the Northern Hemisphere (NH) polar stratosphere in boreal winter indicate a strengthened polar vortex in winters following major tropical volcanic eruptions [*Kodera*, 1995; *Graf et al.*, 2007]. Through stratosphere-troposphere coupling, the signal of a strong NH polar vortex can influence the troposphere, shifting the North Atlantic Oscillation (NAO) to a positive phase [*Baldwin and Dunkerton*, 2001; *Gerber et al.*, 2012] resulting in positive surface temperature anomalies in northern Europe and Siberia as well as negative surface temperature anomalies in the Mediterranean. In posteruption winters, the surface temperature anomaly pattern due to the shift of the NAO to a positive phase is referred to as volcanic winter warming [*Robock and Mao*, 1992; *Robock*, 2000; *Fischer et al.*, 2007; *Christiansen*, 2008].

Different mechanisms have been proposed to explain how tropical volcanic eruptions influence the polar vortex in the NH winter. Large tropical volcanic eruptions can inject substantial amounts of SO_2 in the tropical stratosphere [*Bluth et al.*, 1992; *Textor et al.*, 2004]. Via chemical reactions the SO_2 is converted into sulfate aerosols which absorb solar near-infrared and terrestrial longwave radiation. The absorption of terrestrial and near-infrared radiation leads to heating of the lower stratosphere, which is strongest in the tropics and therefore enhances the meridional temperature gradient [*Labitzke and McCormick*, 1992; *Graf et al.*, 1993; *Kodera*, 1994; *Perlwitz and Graf*, 1995; *Kodera and Kuroda*, 2000]. The thermal wind relation implies that the enhanced meridional temperature gradient strengthens stratospheric westerlies.

Stratospheric warming from volcanic aerosols is, however, largely confined to lower latitudes [*Stenchikov et al.*, 2002; *Toohey et al.*, 2014] and may not have a significant direct effect on the strength of the polar vortex at 60°N, suggesting that other mechanisms may be important. *Stenchikov et al.* [2002] proposed that a weaker meridional temperature gradient in the troposphere, due to maximum radiative cooling of the surface in the tropics [*Robock and Mao*, 1995], leads to a decreased upward planetary wave flux. In normal conditions, the variability of the polar vortex is mainly determined by the wave flux into the stratosphere [*Newman et al.*,

2001; *Polvani and Waugh*, 2004]. A decreased wave flux, as proposed after volcanic eruptions, would logically lead to a stronger and less disturbed polar vortex [*Stenchikov et al.*, 2002]. However, reanalysis data (of a limited sample) show on average an increased wave flux in the two winters following the volcanic eruptions of Agung in 1963, El Chichón in 1982, and Pinatubo in 1991 [*Graf et al.*, 2007], which could be due to the eruptions, the strong El Niño events which have coincided with the eruptions, or internal variability. Modeling results also find enhanced stratospheric wave activity after volcanic aerosol forcing, which impacts the NH high latitudes through strengthening of the stratospheric residual circulation [*Toohey et al.*, 2014]. It remains at present unclear exactly how volcanic forcing impacts wave activity and whether this process might be involved in the expected postvolcanic vortex strengthening.

Whatever the dominant mechanism, model simulations of the dynamical response to large tropical volcanic eruptions leading to the volcanic winter warming pattern remain a challenge. Despite a number of idealized model studies that successfully simulated the dynamical response to volcanic eruptions [*Graf et al.*, 1993; *Kirchner et al.*, 1999; *Rozanov et al.*, 2002], coupled climate models that participated in the Coupled Model Intercomparison Project phases 3 and 5 (CMIP3/CMIP5) show on average a weak dynamical response to large volcanic eruptions compared to observations [*Stenchikov et al.*, 2006; *Driscoll et al.*, 2012; *Charlton-Perez et al.*, 2013]. The CMIP5 multimodel mean reveals a very weak and not significant negative geopotential height anomaly at 50 hPa over northern high latitudes in winter [*Charlton-Perez et al.*, 2013], which corresponds to a minor strengthening of the polar vortex in the first two winters following a tropical eruption. Consequently, the impact on the NAO, the Northern Annular Mode (NAM), and the surface temperatures is small compared to observations and not significant [*Driscoll et al.*, 2012]. Additionally, a well-resolved stratosphere does not improve the dynamical response to volcanic eruptions in the CMIP5 models [*Charlton-Perez et al.*, 2013] in contrast to what has been suggested by earlier studies [*Shindell et al.*, 2004; *Stenchikov et al.*, 2006].

In this study we use the Max Planck Institute Earth system model (MPI-ESM) to further investigate the processes connecting stratospheric volcanic forcing and the NH polar vortex response to better understand the apparent disagreement to observations. We aim to understand the dynamical mechanisms linking volcanic aerosol heating with the NH polar vortex response and focus on the stratospheric response, only. We compare the dynamical response to volcanic aerosol forcing of large-ensemble simulations for two classes of eruptions: Pinatubo-like eruptions and the much stronger 1815 Tambora eruption. We investigate the role of internal variability on the evolution of the NH polar vortex after large tropical volcanic eruptions and thus the robustness of the stratospheric vortex response as a function of the magnitude of volcanic forcing. In section 2 we describe the model and the simulations we performed. The results in section 3 are organized in three parts: first, the zonal mean temperature and the zonal mean zonal wind response to the volcanic eruptions are shown. Second, we focus on the position and strength of the meridional temperature gradient imposed by the eruption. Finally, we investigate the ensemble spread of the stratospheric zonal mean temperatures and zonal winds from the equator to the North Pole. The results are discussed in section 4, followed by a summary and conclusions in section 5.

2. Methods and Data

The MPI-ESM [*Giorgetta et al.*, 2013] is a coupled Earth system model with the atmospheric component ECHAM6 [*Stevens et al.*, 2013], the ocean component Max Planck Institute Ocean Model (MPIOM) [*Jungclaus et al.*, 2013] including the ocean bio-geochemistry model Hamburg Ocean Carbon Cycle Model version 5 (HAMOCC5) [*Ilyina et al.*, 2013], and the land vegetation model JSBACH [*Reick et al.*, 2013]. The configuration used here for all experiments is referred to as "low resolution" (MPI-ESM-LR), meaning a horizontal resolution of the atmospheric component given by a triangular truncation at 63 wave numbers (T63, approximately 1.9°×1.9° at the equator) and 47 vertical layers extending to 0.01 hPa. The ocean has a grid resolution of 1.5°×1.5° (GR1.5) with two poles, one over Antarctica and one over Greenland [*Jungclaus et al.*, 2013]. In this configuration the model does not internally generate the quasi-biennial oscillation (QBO) and dominant easterly winds are simulated in the equatorial stratosphere. The MPI-ESM-LR has been extensively validated and widely used for process and climate-related studies. It reproduces the observed seasonal and interannual stratospheric variabilities [*Charlton-Perez et al.*, 2013], captures the downward propagation of stratospheric signals in the NH winter [*Reichler et al.*, 2012], and simulates the spatial and temporal variabilities of the

NAO as well as the Northern Annular Mode (NAM) [*Driscoll et al.*, 2012; *Cattiaux and Cassou*, 2013] well in comparison with observations. The strength and time scales of the Brewer-Dobson circulation is comparable to reanalysis data [*Bunzel and Schmidt*, 2012; *Schmidt et al.*, 2013]. A detailed description of the responses of the MPI-ESM to anthropogenic and natural forcings in the middle and upper atmosphere is given by *Schmidt et al.* [2013].

We performed a 20-member simulation ensemble of a Tambora-type eruption with the MPI-ESM-LR. The eruption of Tambora took place in April 1815 on the Sanggar Peninsula of Sumbawa Island in Indonesia at 8°S [*Stothers*, 1984]. Estimates of the injected SO_2 are uncertain and range from approximately 50 to 60 Tg [*Self et al.*, 2004; *Gao et al.*, 2008]. In our experiments, the volcanic aerosol forcing is prescribed by a time series of aerosol optical depth (AOD) and effective radius reconstructed from Greenland and Antarctic ice cores [*Crowley et al.*, 2008; *Crowley and Unterman*, 2012]. The Crowley and Unterman data set is one of the two recommended volcanic forcing data sets for the Paleoclimate Modeling Intercomparison Project phase 3 (PMIP3) [*Schmidt et al.*, 2011, 2012]. The AOD time series shows a maximum global mean AOD of the Tambora eruption of approximately 0.4 at 0.55 μm wavelength, corresponding to approximately 55 Tg SO_2 with the AOD-SO_2 conversion rate given by *Gao et al.* [2008]. The time resolution of the volcanic forcing series is 10 days, and the forcing is provided as zonal mean values for four equal-area latitude bands (90°S–30°S, 30°S–0°S, 0°N–30°N, 30°N–90°N). In order to avoid an unphysical step function in the meridional distribution of prescribed AOD in the transition between the tropics and extratropics, the AODs are interpolated between 15° and 45° north and south. This data set shows highest AOD values for the Tambora eruption in the tropical latitude bands and has slightly stronger maximum AOD values in the Southern Hemisphere (SH) than NH ($AOD_{SH}/AOD_{NH} = 1.3$), qualitatively similar to the reconstruction of *Arfeuille et al.* [2014]. The AOD in the model is distributed between 86 and 20 hPa over three stratospheric levels with a maximum at 50 hPa [*Timmreck et al.*, 2009]. The simulations were started from the CMIP5 preindustrial control simulation of the MPI-ESM-LR with constant boundary conditions and greenhouse gas concentrations of the year 1850. Stratospheric ozone concentrations in the historic simulations were prescribed as monthly zonal mean values [*Cionni et al.*, 2011] and do not include variability related to volcanic aerosol. For the preindustrial control simulation, constant monthly mean ozone fields averaged over the years 1850–1860 are used. For each of the 20 ensemble members we chose a different year of the preindustrial control simulation and started the simulation on 1 January of the respective year. The restart dates for the different ensemble members were chosen such that there is no systematic bias toward a specific state of the tropical Pacific and the Atlantic meridional overturning circulation. The eruption was set up in April in accordance with observational records [*Stothers*, 1984]. We analyze the monthly means of the first posteruption winter, and anomalies are calculated for each ensemble member with respect to a 20 year reference period of preindustrial control simulation prior to the chosen eruption year. The statistical significance of anomalies is assessed based on a two-tailed *t* test.

Additionally, we use a 10-member ensemble of CMIP5 historical simulations with the MPI-ESM-LR over the time period of 1850–2005. Volcanic aerosol forcing in the MPI-ESM-LR CMIP5 historical simulations is prescribed by an extended version of the Pinatubo aerosol data set by *Stenchikov et al.* [1998]. This data set is based on measurements of aerosol extinction and derived estimates of effective radii. The data set contains monthly mean zonal averages of the aerosol extinction, single scattering albedo, and asymmetry factor as a function of pressure and wavelength. The latitudinal resolution is 2° from 89°S to 89°N. The data are given at 40 pressure levels and interpolated to the actual hybrid model layers during the simulations. The prescribed AOD forcings at 0.55 μm wavelength are shown in Figure 1a.

We analyze the largest two eruptions of the historical period, the eruptions of Krakatau and Pinatubo. The Krakatau eruption took place in August 1883 on an island between Java and Sumatra, Indonesia, at 6°S [*Rampino and Self*, 1982]. Pinatubo erupted in June 1991 on the Philippine island Luzon at 15°N [*Bluth et al.*, 1992]. As in the Tambora experiment, we calculate anomalies of the posteruption winter by defining volcanically unperturbed reference periods prior to each eruption. Consistent with the Tambora eruption, we select a 20 year reference period for the Krakatau eruption from 1863 to 1882. In the case of the Pinatubo, we can only select 5 years prior to the eruption due to the eruption of El Chichón in 1982. The time mean of each reference period is subtracted from the reference period itself and the first winter after the eruptions to obtain anomalies. In this way we account for the different climatic background states of the Krakatau and Pinatubo eruptions. Anomalies of the posteruption winter months of Krakatau and Pinatubo are calculated with respect to the average of the individual reference periods.

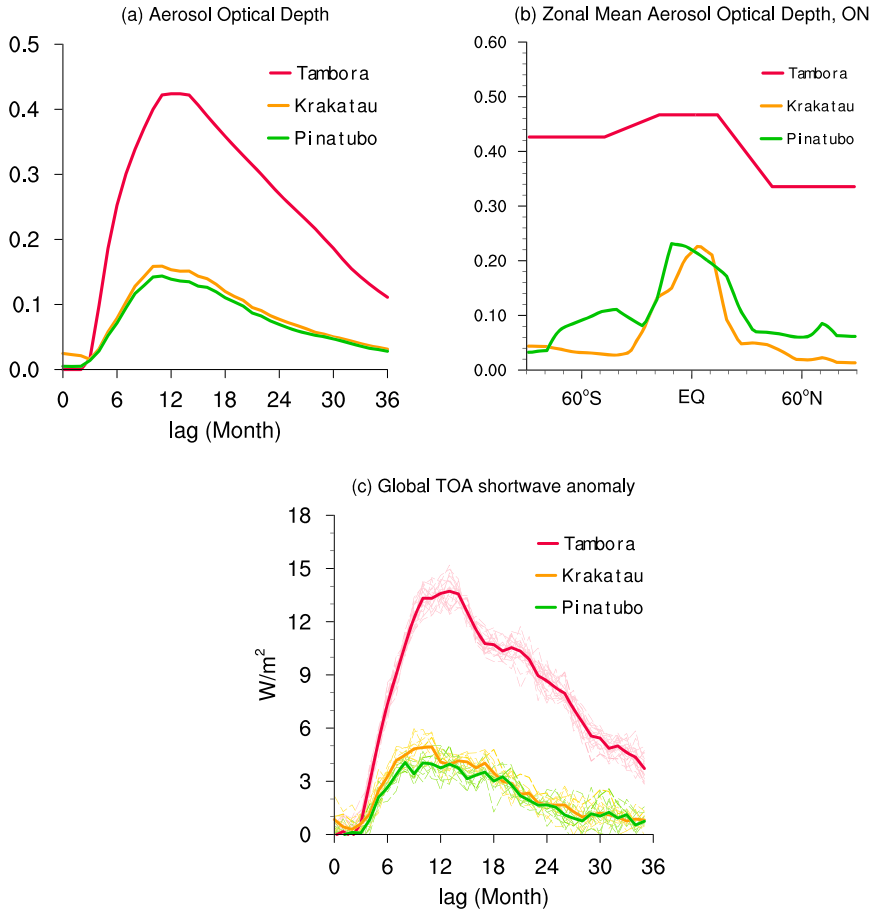

Figure 1. (a) Prescribed global averaged aerosol optical depth (AOD) at 0.55 μm for Tambora (red), Krakatau (orange), and Pinatubo (green). (b) Zonal mean AOD at 0.55 μm in October-November. (c) Simulated anomalies of the global averaged deseasonalized top-of-the-atmosphere (TOA) solar (shortwave) radiation in W/m^2. Thin lines indicate the individual ensembles and thick lines the ensemble average.

Given the very similar magnitude of the Krakatau and Pinatubo eruptions, we combine the simulated responses to the two eruptions into a single 20-member ensemble ("KP" in the following). In the reconstruction of *Sato et al.* [1993], which is the basis of the Stenchikov data set used here, the optical thickness for the Krakatau eruption is 1.1 times that of Pinatubo, and the spatial distribution is the hemispheric mirror image of the satellite-based Pinatubo forcing over the time frame considered in this study (http://data.giss.nasa.gov/modelforce/strataer/), with fairly equal hemispheric partitioning of the AOD. The prescribed monthly mean AOD at 0.55 μm and the simulated global top-of-the-atmosphere (TOA) shortwave anomalies for Krakatau, Pinatubo, and Tambora reveal that even though the radiative forcing and the response of the TOA shortwave anomalies is somewhat larger for the Krakatau eruption compared to the Pinatubo eruption, both quantities are approximately 3–4 times smaller than for the Tambora eruption (Figures 1a and 1c). The zonal mean AOD field of the Tambora eruption is comparable to the spatial structure of the better resolved AOD of the Krakatau and Pinatubo eruptions (Figure 1b). The AOD fields of the Krakatau and Pinatubo are similar with regard to their magnitude as well as the latitudinal AOD gradient, which is strongest between 10°N and 35°N. The ensembles of Krakatau and Pinatubo overlap considerably for the global TOA shortwave anomalies, whereas the Tambora ensemble is well separated (Figure 1c). We therefore assume that the global radiative impact of the Krakatau and the Pinatubo forcing is within the same range to justify combining these two eruptions into a single ensemble of simulations (KP) for the purpose of this study. However, difference in the climatological background states between 1883 and 1991 could be a nonnegligible factor influencing the climatic response to an eruption for surface temperature and ocean dynamics on decadal time scales [*Zanchettin et al.*, 2013]. Nevertheless, we think that for the short-term stratospheric dynamical response, it

can be justified to combine eruptions on different background conditions as it was also done for the assessment of the volcanic response in CMIP3 and CMIP5 simulations [*Stenchikov et al.*, 2006; *Driscoll et al.*, 2012].

Due to our comparably large ensemble and because it is not a priori clear that the mechanisms in the first winter after the eruption are the same as in the second winter, we choose to focus on the first winter after the eruption, only. As we are interested in the seasonal evolution of the winter response, we split the winter season into three parts: early winter (October-November mean), midwinter (December-January mean), and late winter (February-March mean). Further analyzing monthly means does not give qualitatively different results from the seasonal means (not shown). Additionally, we have as model output the diabatic heating rates for the Tambora and the Pinatubo experiments to compare the temperature response after these eruptions to the diabatic forcing of the model.

For comparison of the response to the single eruptions of Tambora, Krakatau, and Pinatubo with the observed response after the Pinatubo eruption, we use the ERA-Interim reanalysis [*Dee et al.*, 2011] from 1980 to 2002. To evaluate the model climatology without volcanic perturbation, we exclude the two winters following the volcanic eruptions of El Chichón in 1982 and the two winters following Pinatubo in 1991.

3. Results

3.1. Temperature and Zonal Wind Response

Observations have suggested that large tropical volcanic eruptions lead to a positive temperature anomaly in the tropical lower stratosphere and an intensification of the polar vortex in NH winter. In the first step, we assess the model performance concerning the zonal mean temperature and zonal wind. We concentrate on the NH only, because we are interested in the dynamical effects on the NH polar vortex.

The Tambora experiment and the KP experiments simulate a significant warming in the tropical lower stratosphere from about 100 hPa up to 10 hPa and from the equator to 60°N during the whole winter following the eruption (Figure 2). The positive temperature anomaly in the equatorial stratosphere in the Tambora experiment is approximately 19 K in early winter and peaks in late winter with approximately 21 K. It is about 4 times larger than in the KP experiments, which show a maximum of about 5 K in late winter, and therefore larger than the AOD ratio between both experiments (Figure 1b). However, the AOD at 0.55 μm is strongly dependent on the particle size. For very strong eruptions such as Tambora, the particle size is larger in the aftermath of the eruption compared to Pinatubo-size eruptions, which lead to a decrease in scattering efficiency [*Timmreck et al.*, 2009]. Hence, one would expect a smaller difference between the Tambora and the Krakatau/Pinatubo eruptions for the AOD at 0.55 μm than for the tropical stratospheric temperature response.

The temperature anomaly of the KP experiments is larger than the observed temperature anomaly after Pinatubo in the winter of 1991/1992 which is in the range of 2–3 K [*Labitzke and McCormick*, 1992]. The difference between the observed and the simulated temperature anomalies cannot fully be explained by the different magnitudes of the Krakatau and the Pinatubo eruptions that are averaged in the KP ensemble. The temperature anomalies in the equatorial stratosphere are approximately only 0.5 K larger after the Krakatau eruption compared to the Pinatubo eruption. However, other sources of variability in the equatorial stratosphere, for instance the QBO and the El Niño–Southern Oscillation (ENSO), or different ozone and water vapor concentrations and feedback mechanisms can alter the temperature response of volcanic eruptions in the real atmosphere [*Ramachandran et al.*, 2000]. *Thomas et al.* [2009b] showed that it is crucial to include all known boundary conditions correctly to simulate the observed equatorial temperature response. They showed in model simulations that the easterly phase of the QBO after the Pinatubo eruption leads to a cooling of 1–2 K at 30 hPa. Because our model setup does not include an internal QBO and does not account for the ozone feedback, and also the AOD forcing fields have substantial uncertainties [*Arfeuille et al.*, 2013], discrepancies to the observed temperature response are expected. In the upper stratosphere/lower mesosphere, a significant negative temperature anomaly in the equatorial region and a significant positive temperature anomaly over the poles occur. Such temperature anomalies have been shown to be due to the acceleration of the residual meridional circulation and the accompanied adiabatic heating anomalies, whereas the contribution of longwave cooling seems to be minor [*Toohey et al.*, 2014]. The maximum of the positive temperature anomaly in the polar upper stratosphere remains during the whole winter at approximately 3–1 hPa. Despite the differences in magnitude, the patterns of the zonal mean temperature anomalies are similar for all experiments.

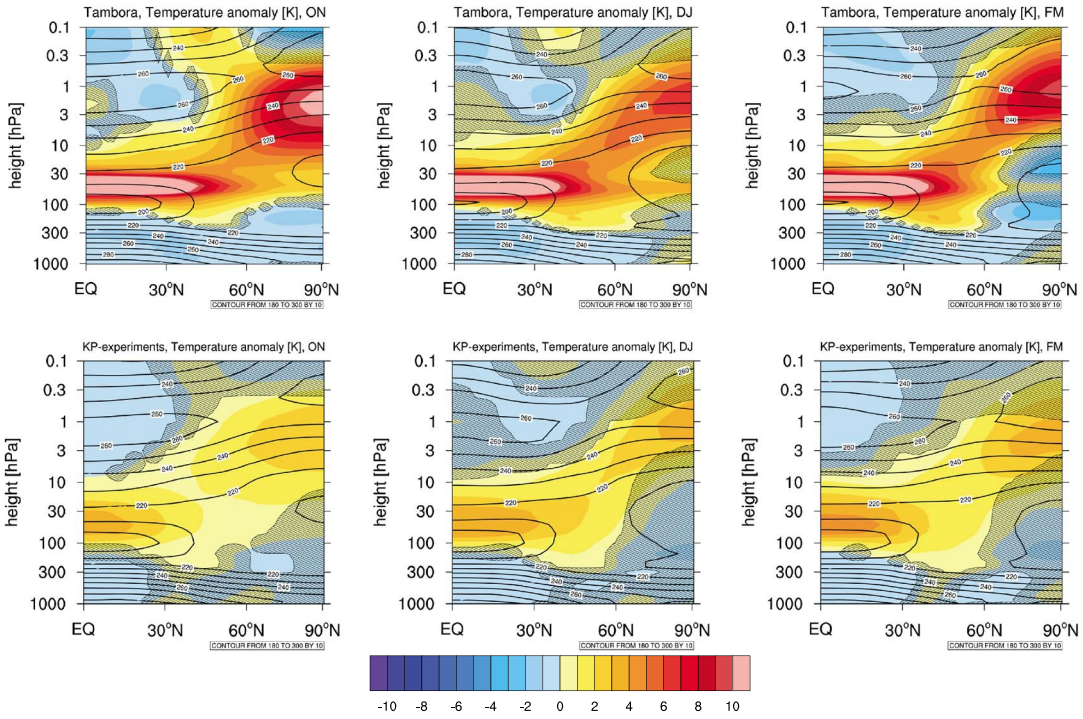

Figure 2. Ensemble average of the zonal mean temperature anomalies (K; colored) averaged over (left) October-November, (middle) December-January, and (right) February-March in the first NH winter for the (top) Tambora and the (bottom) KP experiments. Contour lines display the climatological background conditions of the reference periods. Regions not significant at the 95% confidence level are hatched.

The temperature response is a result of radiative and dynamical feedback processes. The diabatic heating rates due to aerosols (Q^{aer}) and temperature anomalies averaged between 70 hPa and 30 hPa reveal a maximum in the equatorial latitudes (Figure 3). The latitudinal dependence of Q^{aer} is related to the meridional variations in both absorption and emission. Due to relatively high absolute temperatures in the stratosphere in midlatitudes, the emissions dominate, which leads to a local minimum in Q^{aer}. In tropical latitudes, the Q^{aer} is positive because of high absorption of solar and terrestrial radiation and in the polar latitudes because of less emissions due to relatively lower temperatures. These effects are more pronounced in the Tambora simulation compared to the Pinatubo simulation, because of the higher amount of aerosols acting as emitter. Despite the influence of other processes, such as dynamical cooling due to increased upwelling, tropical heating rates and temperature

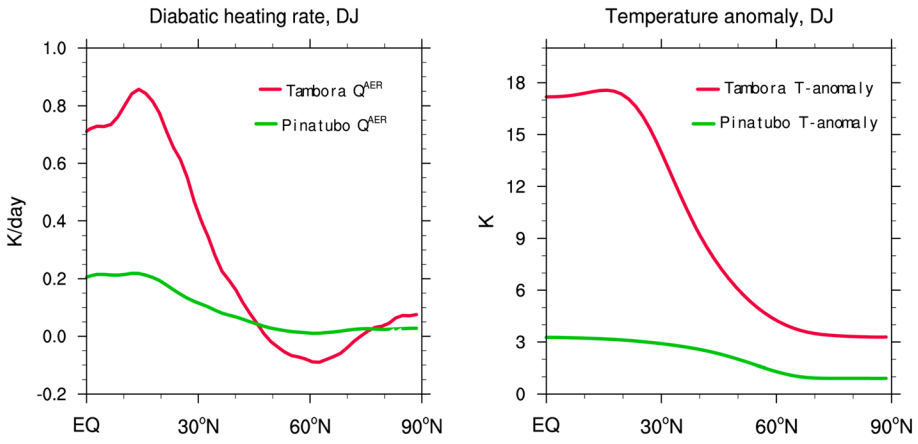

Figure 3. (left) The 70–30 hPa DJ zonally averaged aerosol diabatic heating rates (K/d) in the first NH winter after the eruption of Tambora and Pinatubo. (right) Same as in the left plot but for the zonally averaged mean temperature (K).

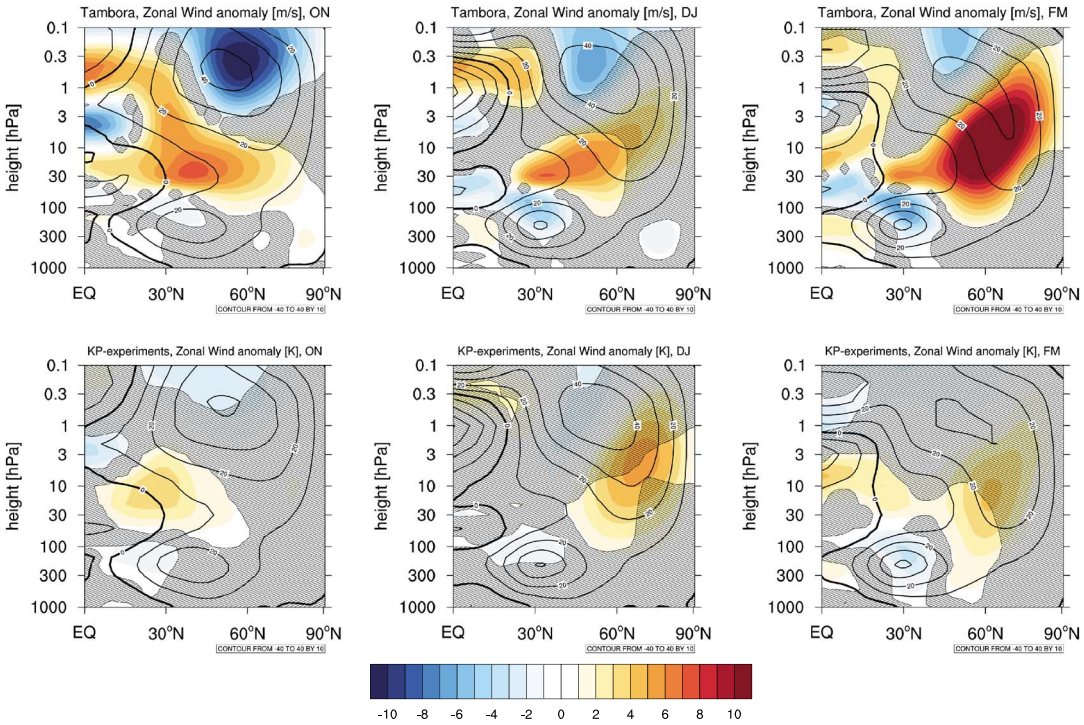

Figure 4. Ensemble average of the zonal mean zonal wind anomalies (m/s; colored) averaged over (left) October-November, (middle) December-January, and (right) February-March in the first NH winter for the (top) Tambora and the (bottom) KP experiments. Positive wind anomalies are defined as eastward. Contour lines display the climatological background conditions of the reference periods. Signals not significant at the 95% confidence level are hatched.

anomalies show qualitative agreement. Hence, we assume that the positive temperature anomaly in the tropical lower stratosphere, as seen in Figure 2, is the original perturbation and is mainly due to the shortwave and longwave radiation absorption by the volcanic aerosols. In the following, we refer to the equatorial temperature anomaly as the direct radiative response of the temperature to volcanic aerosols.

The corresponding zonal mean zonal wind anomalies for the Tambora and the KP experiments show that in the NH, the polar vortex is significantly intensified in late winter of the Tambora experiment (Figure 4). Also, in the KP experiments the NH polar vortex gets stronger, but the signal is only locally significant. However, the magnitude of the intensification of the polar vortex is small compared to observations after the Pinatubo eruption [*Kodera*, 1994] and in large areas not significant. In the context of this study, an important phenomenon is the positive zonal wind anomaly at approximately 30°N at 30 hPa. We interpret this zonal wind anomaly as the direct response of the wind field to the temperature perturbation by the volcanic aerosols. In early winter the positive anomaly is significant in both the Tambora and the KP experiments. In the case of the Tambora experiment, this zonal wind anomaly is persistent during the whole winter, while in the KP experiments it is significant only for early winter. In the upper stratosphere (0.3–1 hPa) in early winter and midwinter, the maximum of the westerly winds is weakened due to the adiabatic heating by the increased meridional circulation (not shown).

3.2. Meridional Temperature Gradient

The vertical change in the zonal wind due to temperature anomalies is dependent on the meridional temperature gradient and, due to the Coriolis force, the latitude. The thermal wind relation implies that the zonal wind changes most where the meridional temperature gradient is steepest. Hence, we focus on the strength and position of the temperature anomaly and the corresponding meridional temperature gradient.

To evaluate the model response, we compare the simulated zonal mean temperature and its meridional gradient with ERA-Interim reanalysis (Figure 5). The model simulates lower temperatures in the subtropics and midlatitudes for the Pinatubo reference period compared with the ERA-Interim volcanically unperturbed state. The temperatures lie outside the natural variability indicated by the ERA-Interim period in early winter, with a

maximum difference of approximately 2 K. Due to the stratospheric cooling by ozone loss and increased anthropogenic greenhouse gases, the zonal mean temperature at 50 hPa is lower for the Pinatubo reference and ERA-Interim periods compared to the preindustrial period of Tambora (Figure 5, top row). The simulated meridional temperature gradient agrees well with the meridional temperature gradient obtained from ERA-Interim (Figure 5, bottom row) and does not exceed the natural variability of the reanalysis data set apart from a very small region around 20°N in midwinter. Hence, we assume that the present model setup is capable of representing the background state of the zonal mean stratospheric temperature reliably.

The heating of the tropical stratosphere due to volcanic aerosols is apparent, because the zonal mean equatorial temperatures after the eruption (dashed lines; Figure 5, top row) are higher compared to their corresponding reference periods (solid lines). For the very large Tambora eruption, the temperature gradient changes sign between 20°N and 40°N (Figure 5, bottom row). Under conditions without volcanic perturbations, the temperature at 50 hPa increases from the equator northward to approximately 50°N and afterward decreases toward the pole. Because the Tambora eruption increases the temperature in low latitudes strongly, the local minimum at the equator disappears.

To identify the response of the zonal mean temperature to the volcanic forcing in more detail, Figure 6 illustrates zonal mean temperature anomalies at the height of the maximum heating in the equatorial region (50 hPa) for the Tambora and KP experiments. The grey shaded area is the ±2 standard deviations (σ) of the preeruption reference period for each experiment. The spread of the grey shaded area indicates the interannual variability of the zonal mean temperature, which is consistently small through the winter in the tropical stratosphere. At polar latitudes, the interannual variability is large compared to the tropics and increases through winter. In the Tambora experiment, the heating due to volcanic aerosols in the tropics leads to a positive zonal mean temperature anomaly of about 20 K from the equator to approximately 25°N. Northward of 25°N the positive zonal mean temperature anomaly decreases, whereas the spread between the ensemble members increases. The positive temperature anomaly of the ensemble mean is significant at the 95% confidence level for all latitudes through winter apart from the polar latitudes in late winter as indicated by the markers at the bottom of the plot. For the KP experiments, the shape of the zonal mean temperature anomalies is similar to the Tambora experiment with positive anomalies from the equator to 30°N and on average zero response in the polar latitudes. The maximum heating in the tropical stratosphere is 15 K smaller than in the Tambora experiment but exceeds the 95% confidence level of the reference period. The spread between the ensemble members in the NH polar winter region, however, is substantial in midwinter and late winter. During this time, some ensemble members show significantly higher polar temperatures, whereas others show the opposite. We will address this issue in more detail in section 3.3.

The thermal wind relation implies that the meridional temperature gradient across the vortex influences the strength of the polar vortex. The meridional temperature anomaly gradient, $\partial T_a/\partial\phi$, where ϕ is the latitude, for the Tambora and the KP experiments (Figure 7) shows negative values for decreasing temperature anomalies from the equator northward. Independent of the eruption magnitude, the strongest ensemble mean meridional temperature anomaly gradient occurs around 30°N, where the heating due to the aerosols gets weaker from the tropics to the poles. For the Tambora experiment, the meridional gradient of every ensemble member at 30°N exceeds the confidence interval during the whole winter. The ensemble mean anomalies are significant from lower latitudes up to 75°N in early winter, 60°N in midwinter, and 70°N in late winter, but the strongest signal can be obtained at extratropical latitudes. In the KP experiments, the maximum meridional gradient at 30°N is considerably smaller compared to the Tambora experiment, but the ensemble mean exceeds the confidence interval from 10°N to 50°N in early winter and late winter and from 10°N to 60°N in midwinter. At 30°N in the extratropical stratosphere, we obtain significant westerly zonal wind anomalies (Figure 4). The most distinct response of the zonal wind field to the meridional temperature anomaly gradient is therefore not a strengthening of the polar vortex but a positive wind anomaly in the subtropical stratosphere.

The positive wind anomaly in the subtropics implies an equatorward shift of the zero-wind line and allows for more equatorward wave propagation. For the case of the large Tambora eruption this is illustrated in Figure 8 by the anomalies of the Eliassen-Palm flux (EP flux) vectors at the location of positive zonal wind anomalies around 30°N. As a consequence, less waves break at high latitudes where the divergence of the EP flux (not shown) and the deceleration of the polar vortex are reduced. Hence, the strengthening of the polar vortex in late winter is not solely an effect of the increased temperature gradient acting directly on the polar vortex but

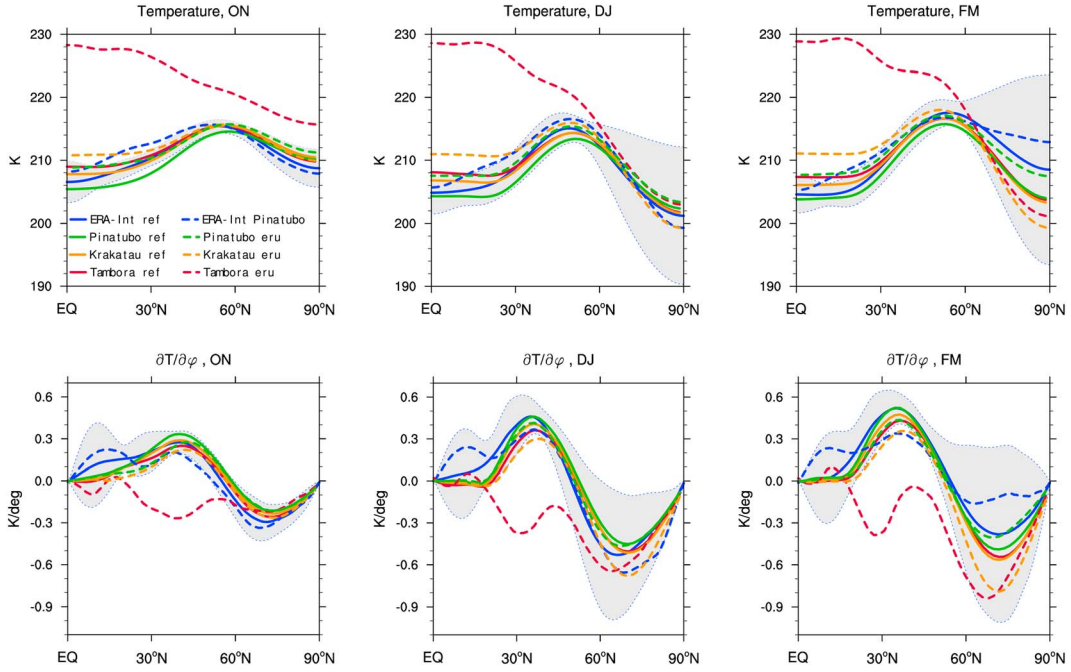

Figure 5. Ensemble averages of the (top) zonal mean temperature (K) and (bottom) temperature gradient (K/deg) at 50 hPa averaged over (left) October-November, (middle) December-January, and (right) February-March. The solid lines show the reference period without volcanic perturbations and the dashed lines the temperature in the NH winter following the respective eruption (red: Tambora; orange: Krakatau; green: Pinatubo). The blue solid line displays the temperature and its gradient averaged over the ERA-Interim period (1980–2001) with 2σ interval (grey shading), and the blue dashed line shows the respective quantities in ERA-Interim after the volcanic eruptions of Pinatubo.

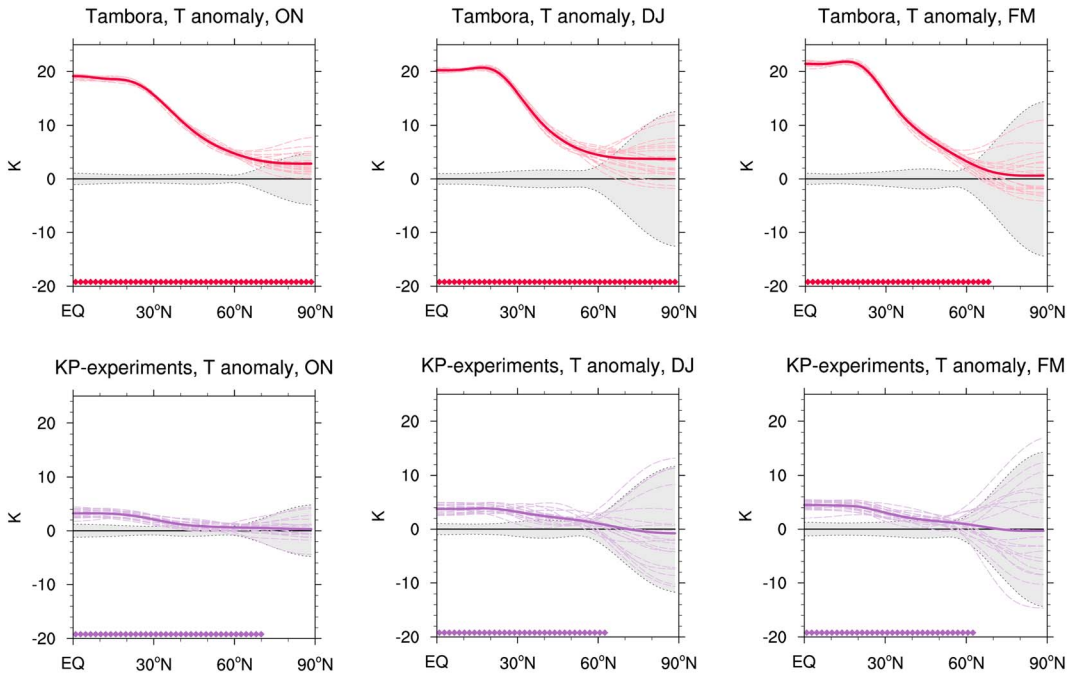

Figure 6. Zonal mean temperature anomalies (K) at 50 hPa averaged over (left) October-November, (middle) December-January, and (right) February-March in the first NH winter for the (top) Tambora and the (bottom) KP experiments. The thin dashed lines are the individual ensemble members, and the thick solid line is the ensemble average. The grey shading displays the 2σ interval of the reference period of the respective experiment, and the bottom dots indicate whether the ensemble mean is significantly different from the reference period.

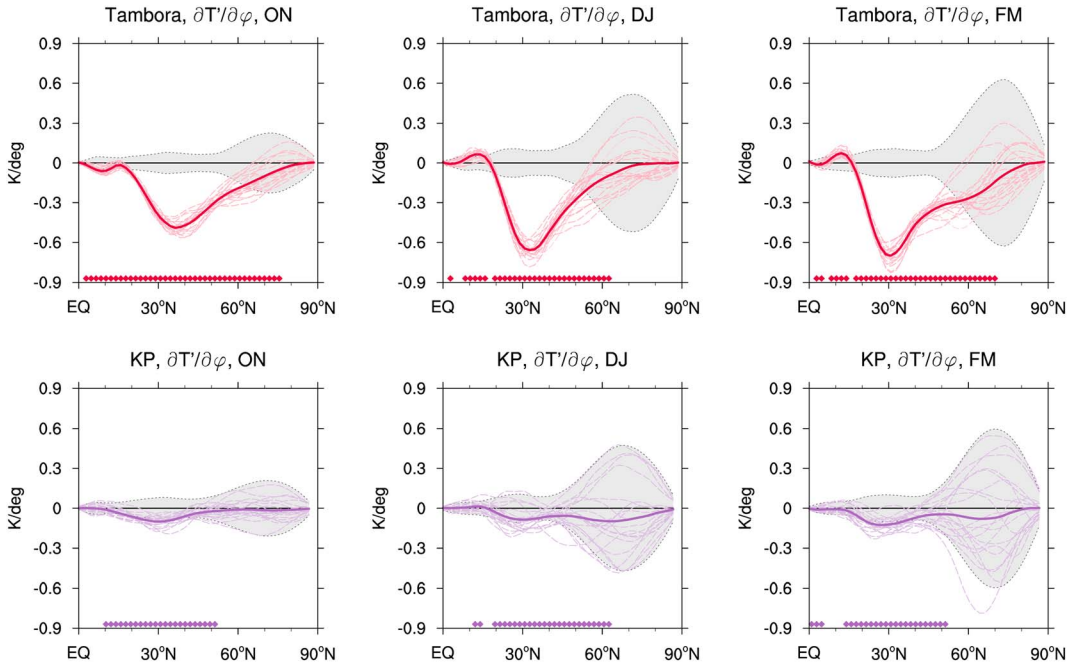

Figure 7. Same as in Figure 6 but for the zonal mean temperature anomaly gradient (K/deg) at 50 hPa.

rather an indirect effect due to a changed propagation of planetary waves. We obtain a similar behavior of the EP flux for the KP experiments in early winter, but because the magnitude of the original zonal wind perturbation is smaller compared to the Tambora experiment, the change of the EP flux is also small. In midwinter and late winter, where there is not a strong change of the zonal mean zonal wind at approximately 30°N, the EP flux does not show significant response (not shown). It appears that because the original temperature anomaly only weakly affects the polar vortex directly, the response of the polar vortex is less robust. Still, this newly identified dynamical mechanism works for both eruptions magnitudes and links the original temperature perturbation in the tropical stratosphere via changes in the temperature gradient and subsequent zonal wind anomaly around 30°N to the strengthening of the NH polar vortex. Hence, the polar vortex intensification is not a result of a direct impact of the increased meridional temperature gradient in the stratosphere but an indirect effect due to the equatorward deflection of planetary waves.

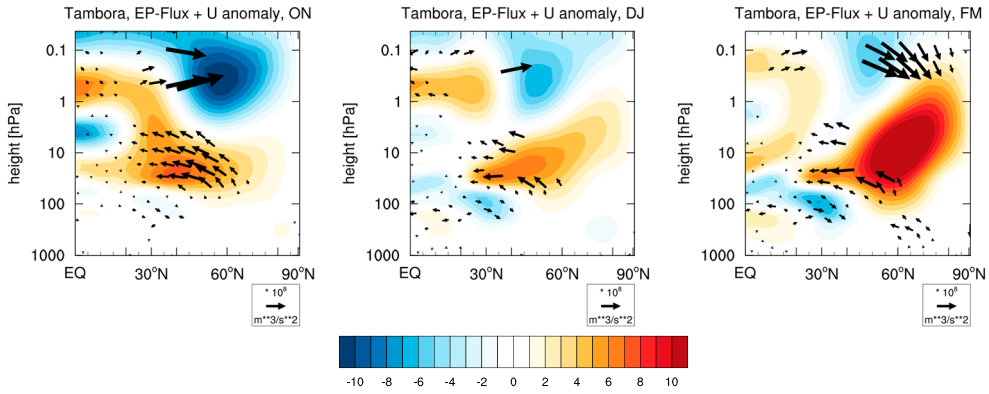

Figure 8. Shaded regions display the ensemble average zonal mean zonal wind anomalies (m/s) averaged over (left) October-November, (middle) December-January, and (right) February-March in the first NH winter after the Tambora eruption (same as in Figure 4, top row). Arrows show the ensemble average Eliassen-Palm flux (m^3/s^2). Only vectors which are significant at the 95% confidence level are shown. For better visibility, the EP flux vector is scaled by division through the density ρ_0 [*Andrews et al.*, 1987].

3.3. Ensemble Variability

In this section we investigate to what extent a tropical eruption influences the posteruption ensemble variability of the polar stratosphere. We use the 50 hPa zonal mean temperature anomaly in the first year after the eruption and calculate the standard deviation of the 20 ensemble members for the Tambora and KP experiments. The interannual variability of the unperturbed stratosphere is quantified by the standard deviation of 20 randomly chosen years of the preindustrial control simulation and the preeruption reference period for comparison with the eruption experiments. We repeat this resampling process 1000 times and average over the standard deviations of the unperturbed stratosphere. The standard deviation of the ERA-Interim period, excluding winters influenced by volcanic eruptions, is also shown for reference (Figure 9, bottom row). The unperturbed stratosphere of all experiments shows weak interannual variability in early winter at high latitudes. The interannual variability increases over the course of the winter reaching up to 7.5 K in late winter. Differences between the model and the reanalysis data occur in the tropics and midlatitudes, where the reanalysis shows stronger interannual variability compared to the model. This can be explained by the absence of the QBO in the model, which dominates the variability in the tropical stratosphere [*Baldwin et al.*, 2001]. At polar latitudes the MPI-ESM-LR captures the observed interannual variability throughout the winter well.

For the Tambora experiment, we obtain significantly weaker ensemble variability in the equatorial stratosphere during the whole winter (Figure 9, top row) compared to the unperturbed variability. The diabatic heating of the volcanic aerosols reduces the ensemble variability, at least in the absence of the QBO. Striking is the significantly reduced ensemble variability in the northern polar stratosphere from midwinter onward. Even though we do not obtain significantly lower or higher temperatures in this region in late winter, the decreased variability suggests that the polar stratosphere is constrained to a state with stronger than average zonal winds. The KP experiments exhibit two remarkable differences compared to the Tambora experiment (Figure 9, bottom row). First, the ensemble variability in the tropical stratosphere is not reduced compared to the control variability. The weak increase is related to the slightly different AOD values between the Krakatau and the Pinatubo experiments, which lead to slightly different temperature anomalies between the Krakatau and the Pinatubo eruptions. Second, the ensemble variability of the 50 hPa temperature anomaly at middle and high latitudes is not decreased but increased compared to the unperturbed stratosphere.

To investigate the response of the polar vortex to the applied forcing, we show the variability anomalies of the zonal mean zonal wind. We subtracted the interannual variability of the volcanically unperturbed period from the ensemble variability of the Tambora and KP experiments at all pressure levels. We do not find any significant responses in the NH polar region in early winter, but midwinter and late winter show a similar response (late winter shown in Figure 10). A significant reduction of the polar vortex zonal mean zonal wind variability is apparent in the Tambora experiment, which confirms the findings of the zonal mean temperature variability at 50 hPa in Figure 9. The reduced variability is significant between 100 hPa and 3 hPa north of 60°N. The variability anomalies of the zonal mean zonal wind of the KP experiments show the opposite response, with increased variability in the region of the polar vortex. However, the signal is slightly shifted equatorward and only significant in a small region between 100 hPa and 30 hPa at 60°N. The increase in variability in the KP ensemble is not due to the merging of the Krakatau and Pinatubo eruptions, because we find a similar behavior if we consider the eruptions separately. With the available data, it is not possible to explain the increased variability. Nevertheless, the different behavior of the Tambora and KP experiments, especially the reduced variability of the Tambora ensemble, indicates that only the very strong Tambora forcing produces a robust stronger-than-average NH polar vortex.

The increased ensemble variability in the KP experiments in the NH polar stratosphere with respect to the interannual variability of the unperturbed reference period helps to explain the limited significance of the response of climate models to volcanic eruptions in the CMIP5 historical period. Our results show that at least the MPI-ESM-LR is able to reproduce the intensification of the polar vortex, as expected based on observations, using the very strong Tambora forcing. In contrast to the Tambora simulations, the Krakatau and Pinatubo forcings, in this model setup, do not robustly force the polar stratosphere into a state of a stronger vortex. Even if the ensemble average does suggest an intensified polar vortex, the impact of the volcanic

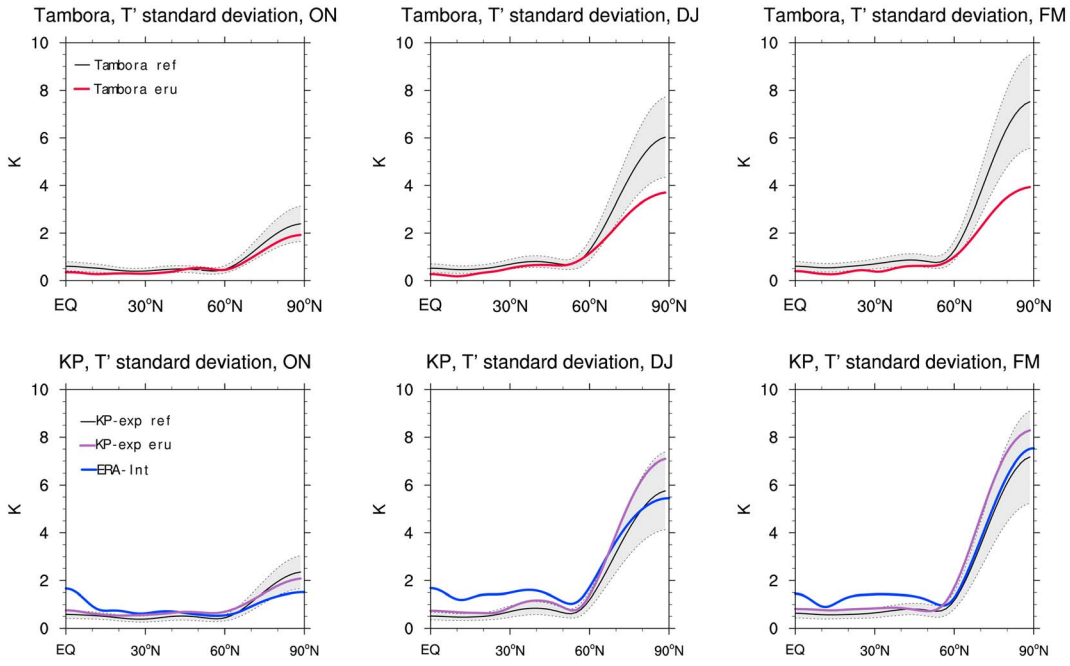

Figure 9. Standard deviation of the 50 hPa zonal mean temperature anomalies (K) averaged over (left) October-November, (middle) December-January, and (right) February-March in the first NH winter for the (top) Tambora and the (bottom) KP experiments. The solid black line displays the averaged standard deviation of a 20-member ensemble randomly drawn 1000 times out of the reference period with the grey shading as 2σ interval. The blue solid line in the bottom plots shows the 50 hPa zonal mean temperature standard deviation of the ERA-Interim period excluding years with volcanic eruptions.

eruption is not discernable from the internal variability of the polar NH stratosphere. For smaller eruptions compared to Tambora, like Krakatau or Pinatubo, the model internal variability masks the response to the forcing of the volcanic aerosols. The reason for this masking is twofold: first, the MPI-ESM-LR shows a slightly too large interannual variability compared to observations in early winter. This overestimation of variability might well have an impact on the evolution of the polar vortex in midwinter and late winter. Second, the polar vortex in the MPI-ESM-LR seems to be relatively insensitive also to other forcings like the QBO, solar variability, or ENSO [*Schmidt et al.*, 2013].

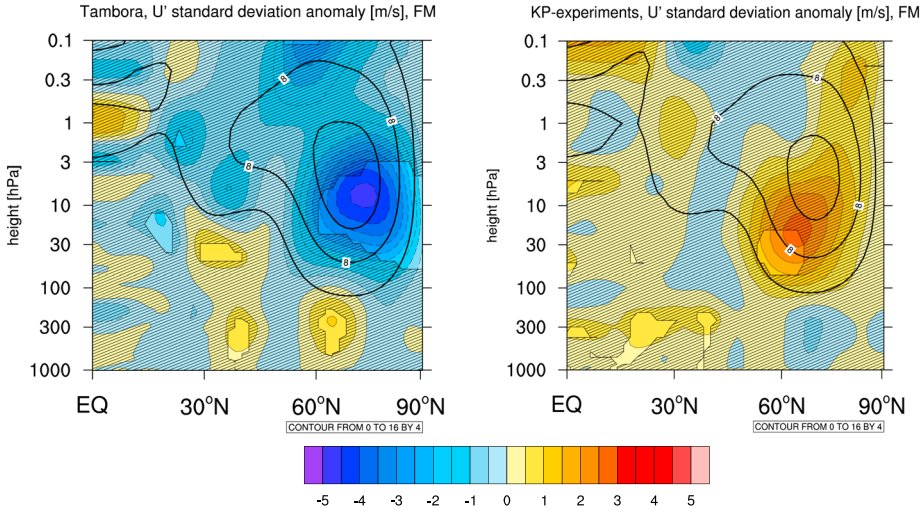

Figure 10. Standard deviation anomalies of the zonal mean zonal wind anomalies (m/s; colored) averaged over February-March in the first NH winter for the (left) Tambora and the (right) KP experiments. Contour lines display the climatological background conditions of the reference periods. Signals not significant at the 2σ level are hatched.

4. Discussion

A key result of our study is that the mechanism leading to a strengthened polar vortex after large tropical volcanic eruptions starts with an anomaly of the zonal mean zonal wind in the stratosphere at 30°N in early winter. This result agrees with previous studies which show that the stratospheric radiative forcing from tropical volcanic aerosols is confined to lower latitudes and does not act directly on the polar vortex [*Stenchikov et al.*, 2002; *Toohey et al.*, 2014]. The multimodel mean of 15 different CMIP5 models shows a positive zonal wind anomaly in this region in ON as well, which indicates that the proposed mechanism might not just be a feature of the MPI-ESM-LR (see supporting information). Zonal wind anomalies in the extratropical stratosphere change the background conditions for the propagation of tropospheric planetary waves [*Shepherd and McLandress*, 2011]. Because the variability of the polar vortex strength is largely controlled by planetary wave drag [*Newman et al.*, 2001; *Polvani and Waugh*, 2004], changes of the background conditions for planetary waves to propagate into the stratosphere will have an impact on the polar vortex [*Charney and Drazin*, 1961]. Several phenomena remote from the polar stratosphere itself, such as ENSO [*van Loon and Labitzke*, 1987; *Manzini et al.*, 2006; *Garfinkel and Hartmann*, 2007], the QBO [*Holton and Tan*, 1980; *Labitzke and Van Loon*, 1988], or the 11 year solar cycle [*Kodera and Kuroda*, 2000], can alter the propagation of planetary waves and thereby impact the evolution of the polar vortex. However, the combination of these forcing factors may not be linear [*Camp and Tung*, 2007; *Calvo et al.*, 2009] and subject to sampling biases [*Thomas et al.*, 2009a; *Graf et al.*, 2014]. Because of the relatively short record of stratospheric observations, the effect of volcanic eruptions on the polar vortex is especially hard to distinguish from internal variability. In particular, the coincidence of El Niño events and large tropical volcanic eruptions aggravates the problem of the limited number of volcanic eruptions in the observational period [*Thomas et al.*, 2009a]. In the Tambora experiment, our results are not biased through an accidental prevalence of a specific ENSO phase in the ensemble. We find a slight domination of La Niña phases in the ensemble of the KP experiments, but we expect that this small bias does not impact our results qualitatively. Furthermore, it has been suggested by model studies that the phase of the QBO might impact the response of the polar vortex to tropical volcanic eruptions [*Stenchikov et al.*, 2004; *Thomas et al.*, 2009a, 2009b]. The QBO changes the propagation of planetary waves and might therefore influence the dynamical mechanism proposed in this study. However, the background zonal mean zonal wind at 30°N between 30 hPa and 10 hPa is in our simulations of similar magnitude compared to the zonal mean zonal wind in reanalysis data in both phases of the QBO [*Pascoe et al.*, 2005]. Hence, we assume that the deflection of planetary waves due to the volcanically induced zonal mean zonal wind anomaly in stratosphere at 30°N is qualitatively independent of the phase of the QBO. Still, the deflection of planetary waves could be enhanced or damped depending on the QBO phase, which would need to be tested in dedicated experiments.

There is some evidence that the spatiotemporal structure of the prescribed aerosol forcing may affect the stratospheric dynamical response [*Toohey et al.*, 2014], which might call into question the accuracy of the forcings used here. The AOD forcing field used for the Tambora experiments is of much cruder horizontal resolution compared to the forcing fields used for the Krakatau and Pinatubo eruptions. However, as we have shown in Figure 1b, the position of the zonal mean AOD gradient of the Tambora eruption is in reasonable agreement with the position of the gradient for the finer resolved Krakatau and Pinatubo eruptions. The position of the strongest meridional temperature anomaly gradient and the positive zonal mean zonal wind anomaly at 30°N in the KP experiments are also obtained if we consider Krakatau and Pinatubo separately. The temperature anomaly gradients for Krakatau and Pinatubo are similar during the winter compared to the strong Tambora eruption. These results suggest that at least qualitatively, the meridional temperature gradient and zonal wind response at 30°N in early winter are unlikely to be significantly sensitive to minor differences in forcing structure. Furthermore, the spatial pattern of the AOD may depend on the exact latitude and season of the eruption [*Toohey et al.*, 2013; *Sigl et al.*, 2014], but as all three eruptions take place in spring/summer season, we assume that the influence of the season is not significant for the processes we investigated in this study. The position of the meridional AOD gradient in the Tambora and KP experiments agrees with satellite measurements after the tropical Pinatubo eruption which showed that the aerosols cloud was bounded between 20°S and 30°N in the tropical stratosphere [*McCormick and Veiga*, 1992; *Trepte and Hitchman*, 1992; *Trepte et al.*, 1993]. Moreover, also satellite measurements after the Pinatubo eruption suffer from uncertainties which are due to gaps in the satellite record from sparse sampling of the satellite instrument [*Stenchikov et al.*, 1998]. Updates to the retrieval of the satellite products have led to significant changes in the

space-time morphology of the estimated aerosol extinction after the Pinatubo eruption, and a new forcing set has been made available [*Arfeuille et al.*, 2013]. A comparison between the data set used here and the new forcing set by *Arfeuille et al.* [2013] was carried out in the study by *Toohey et al.* [2014], where they did not find a significant difference in the NH winter polar vortex response between these two forcing data sets.

The polar vortex may not only respond to changes in the wave drag after volcanic eruptions but can also be influenced by chemical processes. Observation after the Pinatubo eruption showed a substantial ozone depletion [*Newman et al.*, 1997; *Solomon*, 1999; *Tabazadeh et al.*, 2002], which can contribute to a colder polar stratosphere and hence a stronger NH polar vortex in the following winter [*Stenchikov et al.*, 2002]. However, *Marshall et al.* [2009] pointed out that ozone chemistry is unlikely to be a major factor in the NH dynamical response to tropical volcanic eruptions before the most recent decades, because ozone depletion can only be important if ozone-destroying chlorine is abundant in the stratosphere. Still, a modeling study by *Muthers et al.* [2014] with a coupled atmosphere-ocean model shows that for a Tambora-like eruption the influence of different ozone climatologies on the NH winter warming is significant. With our model setup it is not possible to quantify the impact of ozone on the tropical and high-latitude temperature anomalies.

We find a strong positive wind anomaly in the Southern Hemisphere (SH) middle and upper stratosphere during austral summer season for both experiments (see supporting information), which is not apparent in reanalysis data. The reason for this discrepancy is unclear, but from the thermal wind theoretical arguments, a westerly zonal wind anomaly in both hemispheres would be expected. The multimodel average of the CMIP5 models shows a positive wind anomaly in the SH stratosphere in a comparable magnitude to the MPI-ESM-LR (see supporting information). The discrepancy between the model results and the reanalysis data may be related to the strong anomalous wave activity observed in the SH after the Pinatubo eruption [*Schnadt Poberaj et al.*, 2011] but may also be due to the discussed shortcomings of the model, such as the lack of a QBO or missing ozone feedback mechanisms. Still, the mechanisms which are important for the austral summer response of the stratosphere to tropical volcanic eruptions are not well understood and should be addressed in future research.

As outlined in the Introduction, coupled climate models fail to reproduce on average the robustly observed shift of the NAO to a positive phase after large tropical volcanic eruptions, at least if the two winters after each eruption are considered [*Driscoll et al.*, 2012]. Our study focuses on the stratospheric response. Nevertheless, an analysis of the sea level pressure (SLP) anomalies after the Tambora and KP experiments has been conducted. For the KP experiments, changes of the mean SLP in the North Atlantic do not project onto the NAO in December-January-February. Because it has been shown that the MPI-ESM-LR can reproduce the stratospheric-tropospheric coupling [*Reichler et al.*, 2012], this might indicate that the mean polar vortex anomaly in the KP experiments is too weak to significantly influence the troposphere. For the Tambora experiment, where the strongest amplification of the NH polar vortex is simulated in late winter, we find a positive SLP anomaly slightly north of the Azores and a negative SLP anomaly north of Iceland in March-April. Thus, a slight shift to a positive phase of the NAO, as observed after large tropical volcanic eruptions, can be deduced.

5. Summary and Conclusions

We investigated the impact of large tropical volcanic eruptions on the NH polar stratosphere in the MPI-ESM-LR. We compared two model ensembles of different eruption strength and focus on the first posteruption winter. One 20-member ensemble of simulations covers the large Tambora eruption, and a second ensemble (KP experiments) consists of a combined 20-member ensemble of 10 Krakatau eruptions and 10 Pinatubo eruptions.

All model experiments reveal the expected positive zonal mean temperature anomalies in the equatorial stratosphere due to the absorption of radiation by the volcanic aerosols. The temperature anomalies in this region are 4 times larger after the Tambora eruption compared to the KP eruptions. The zonal wind anomalies show after the Tambora eruption a significant intensification of the polar vortex in late winter. After the smaller KP eruptions, the strengthening of the polar vortex is weak, and in large areas not significant.

We focused on two important factors to explain the different results of the Tambora experiment compared to the KP experiments: first, the position of the maximum meridional temperature gradient after a volcanic eruption and second, the volcanically induced effect on the ensemble spread of the NH stratospheric temperature anomalies. Our main results are summarized as follows:

1. The strongest change of the temperature gradient is not in the region of the polar vortex but occurs equatorward at approximately 30°N. Consequently, we find significant zonal wind anomalies in both experiments at 30°N between 30 hPa and 10 hPa in early winter.
2. We have identified a dynamical mechanism that links the subtropical gradient in the heating rate anomaly with the strength of the polar vortex. The positive wind anomaly at 30°N changes the background condition for wave propagation, leading to a deflection of planetary waves to lower latitudes. Waves deposit less momentum in the region of the NH polar vortex, and therefore the wave-driven deceleration of the zonal wind at high latitudes is hampered.
3. We find a reduced ensemble spread in the Northern Hemisphere polar stratosphere for the very large Tambora eruption, which implies that the model is forced to a state of a significantly stronger NH polar vortex.

For the smaller eruptions of Pinatubo and Krakatau, the increased meridional temperature gradient only weakly influences the polar vortex directly and the indirect effect by the deflection of waves toward lower latitudes is less robust. The large spread between the individual ensemble members of the KP simulations reveals that internal variability plays a dominant role for the state of the polar vortex in the posteruption winter. To what extent the indirect effect acts in the real atmosphere is hard to quantify, because of the lack of stratospheric observations after large tropical volcanic eruptions and because other sources of variability, for instance the QBO and ENSO, alter the proposed mechanism of the deflection of planetary waves. Further research should hence be directed into the wave-mean flow interactions after volcanic eruptions.

Acknowledgments
This work was supported by the Federal Ministry for Education and Research in Germany through the research program "MiKlip" (FKZ: 01LP130A (M.B. and C.T.)/ 01LP1130B (M.T.)). Computations were done at the German Climate Computing Center. We thank Davide Zanchettin who did the internal review at MPI and Rabea Athmer who contributed to the simulation of the Tambora experiment as well as three anonymous reviewers who gave contructive comments on an earlier version of the manuscript. Primary data and scripts used in the analysis and other supporting information that may be useful in reproducing the author's work are archived by the Max Planck Institute for Meteorology and can be obtained by contacting publications@mpimet.mpg.de

References

Andrews, D. G., J. R. Holton, and C. B. Leovy (1987), *Middle Atmosphere Dynamics*, Academic Press, San Diego, Calif.

Arfeuille, F., B. P. Luo, P. Heckendorn, D. Weisenstein, J. X. Sheng, E. Rozanov, M. Schraner, S. Brönnimann, L. W. Thomason, and T. Peter (2013), Modeling the stratospheric warming following the Mt. Pinatubo eruption: Uncertainties in aerosol extinctions, *Atmos. Chem. Phys.*, *13*(22), 11,221–11,234, doi:10.5194/acp-13-11221-2013.

Arfeuille, F., D. Weisenstein, H. MacK, E. Rozanov, T. Peter, and S. Brönnimann (2014), Volcanic forcing for climate modeling: A new microphysics-based data set covering years 1600-present, *Clim. Past*, *10*, 359–375, doi:10.5194/cp-10-359-2014.

Baldwin, M. P., and T. J. Dunkerton (2001), Stratospheric harbingers of anomalous weather regimes, *Science*, *294*(5542), 581–584, doi:10.1126/science.1063315.

Baldwin, M. P., et al. (2001), The quasi-biennial oscillation, *Rev. Geophys.*, *39*(2), 179–229, doi:10.1029/1999RG000073.

Bluth, G. J. S., S. D. Doiron, C. C. Schnetzler, A. J. Krueger, and L. S. Walter (1992), Global tracking of the SO_2 clouds from the June, 1991 Mount Pinatubo eruptions, *Geophys. Res. Lett.*, *19*(2), 151–154, doi:10.1029/91GL02792.

Bunzel, F., and H. Schmidt (2012), The Brewer-Dobson circulation in a changing climate: Impact of the model configuration, *J. Atmos. Sci.*, *70*(5), 1437–1455.

Calvo, N., M. A. Giorgetta, R. Garcia-Herrera, and E. Manzini (2009), Nonlinearity of the combined warm ENSO and QBO effects on the Northern Hemisphere polar vortex in MAECHAM5 simulations, *J. Geophys. Res.*, *114*, D13109, doi:10.1029/2008JD011445.

Camp, C. D., and K.-K. Tung (2007), The influence of the solar cycle and QBO on the late-winter stratospheric polar vortex, *J. Atmos. Sci.*, *64*(4), 1267–1283, doi:10.1175/JAS3883.1.

Cattiaux, J., and C. Cassou (2013), Opposite CMIP3/CMIP5 trends in the wintertime Northern Annular Mode explained by combined local sea ice and remote tropical influences, *Geophys. Res. Lett.*, *40*, 3682–3687, doi:10.1002/grl.50643.

Charlton-Perez, A. J., et al. (2013), On the lack of stratospheric dynamical variability in low-top versions of the CMIP5 models, *J. Geophys. Res. Atmos.*, *118*, 2494–2505, doi:10.1002/jgrd.50125.

Charney, J. G., and P. G. Drazin (1961), Propagation of planetary-scale disturbances from the lower into the upper atmosphere, *J. Geophys. Res.*, *66*(1), 83–109, doi:10.1029/JZ066i001p00083.

Christiansen, B. (2008), Volcanic eruptions, large-scale modes in the Northern Hemisphere, and the El Niño–Southern Oscillation, *J. Clim.*, *21*(5), 910–922, doi:10.1175/2007JCLI1657.1.

Cionni, I., V. Eyring, J. F. Lamarque, W. J. Randel, D. S. Stevenson, F. Wu, G. E. Bodeker, T. G. Shepherd, D. T. Shindell, and D. W. Waugh (2011), Ozone database in support of CMIP5 simulations: Results and corresponding radiative forcing, *Atmos. Chem. Phys.*, *11*(21), 11,267–11,292, doi:10.5194/acp-11-11267-2011.

Crowley, T. J., and M. B. Unterman (2012), Technical details concerning development of a 1200-yr proxy index for global volcanism, *Earth Syst. Sci. Data Discuss.*, *5*, 1–28, doi:10.5194/essdd-5-1-2012.

Crowley, T. J., G. Zielinski, B. Vinther, R. Udisti, K. Kreutz, J. Cole-Dai, and E. Castellano (2008), Volcanism and the Little Ice Age, *PAGES News*, *16*(2), 22–23.

Dee, D. P., et al. (2011), The ERA-Interim reanalysis: Configuration and performance of the data assimilation system, *Q. J. R. Meteorol. Soc.*, *137*(656), 553–597, doi:10.1002/qj.828.

Driscoll, S., A. Bozzo, L. J. Gray, A. Robock, and G. Stenchikov (2012), Coupled Model Intercomparison Project 5 (CMIP5) simulations of climate following volcanic eruptions, *J. Geophys. Res.*, *117*, D17105, doi:10.1029/2012JD017607.

Fischer, E. M., J. Luterbacher, E. Zorita, S. F. B. Tett, C. Casty, and H. Wanner (2007), European climate response to tropical volcanic eruptions over the last half millennium, *Geophys. Res. Lett.*, *34*, L05707, doi:10.1029/2006GL027992.

Gao, C., A. Robock, and C. Ammann (2008), Volcanic forcing of climate over the past 1500 years: An improved ice core-based index for climate models, *J. Geophys. Res.*, *113*, D23111, doi:10.1029/2008JD010239.

Garfinkel, C. I., and D. L. Hartmann (2007), Effects of the El Niño–Southern Oscillation and the quasi-biennial oscillation on polar temperatures in the stratosphere, *J. Geophys. Res.*, *112*, D19112, doi:10.1029/2007JD008481.

Gerber, E. P., et al. (2012), Assessing and understanding the impact of stratospheric dynamics and variability on the Earth system, *Bull. Am. Meteorol. Soc.*, *93*(6), 845–859, doi:10.1175/BAMS-D-11-00145.1.

Giorgetta, M. A., et al. (2013), Climate and carbon cycle changes from 1850 to 2100 in MPI-ESM simulations for the Coupled Model Intercomparison Project phase 5, *J. Adv. Model. Earth Syst.*, *5*, 572–597, doi:10.1002/jame.20038.
Graf, H.-F., I. Kirchner, A. Robock, and I. Schult (1993), Pinatubo eruption winter climate effects: Model versus observations, *Clim. Dyn.*, *9*(2), 81–93, doi:10.1007/BF00210011.
Graf, H.-F., Q. Li, and M. A. Giorgetta (2007), Volcanic effects on climate: Revisiting the mechanisms, *Atmos. Chem. Phys.*, *7*(17), 4503–4511, doi:10.5194/acp-7-4503-2007.
Graf, H.-F., D. Zanchettin, C. Timmreck, and M. Bittner (2014), Observational constraints on the tropospheric and near-surface winter signature of the Northern Hemisphere stratospheric polar vortex, *Clim. Dyn.*, 1–22, doi:10.1007/s00382-014-2101-0.
Holton, J. R., and H.-C. Tan (1980), The influence of the equatorial quasi-biennial oscillation on the global circulation at 50 mb, *J. Atmos. Sci.*, *37*(10), 2200–2208, doi:10.1175/1520-0469(1980)037%3C2200:TIOTEQ%3E2.0.CO;2.
Ilyina, T., K. D. Six, J. Segschneider, E. Maier-Reimer, H. Li, and I. Núñez-Riboni (2013), Global ocean biogeochemistry model HAMOCC: Model architecture and performance as component of the MPI-Earth system model in different CMIP5 experimental realizations, *J. Adv. Model. Earth Syst.*, *5*(2), 287–315, doi:10.1029/2012MS000178.
Jungclaus, J. H., N. Fischer, H. Haak, K. Lohmann, J. Marotzke, D. Matei, U. Mikolajewicz, D. Notz, and J. S. von Storch (2013), Characteristics of the ocean simulations in the Max Planck Institute Ocean Model (MPIOM), the ocean component of the MPI-Earth system model, *J. Adv. Model. Earth Syst.*, *5*(2), 422–446, doi:10.1002/jame.20023.
Kirchner, I., G. L. Stenchikov, H.-F. Graf, A. Robock, and J. C. Antuña (1999), Climate model simulation of winter warming and summer cooling following the 1991 Mount Pinatubo volcanic eruption, *J. Geophys. Res.*, *104*(D16), 19,039–19,055, doi:10.1029/1999JD900213.
Kodera, K. (1994), Influence of volcanic eruptions on the troposphere through stratospheric dynamical processes in the Northern Hemisphere winter, *J. Geophys. Res.*, *99*(D1), 1273–1282, doi:10.1029/93JD02731.
Kodera, K. (1995), On the origin and nature of the interannual variability of the winter stratospheric circulation in the Northern Hemisphere, *J. Geophys. Res.*, *100*(D7), 14,077–14,087, doi:10.1029/95JD01172.
Kodera, K., and Y. Kuroda (2000), Tropospheric and stratospheric aspects of the Arctic Oscillation, *Geophys. Res. Lett.*, *27*, 3349–3352, doi:10.1029/2000GL012017.
Labitzke, K., and M. P. McCormick (1992), Stratospheric temperature increases due to Pinatubo aerosols, *Geophys. Res. Lett.*, *19*(2), 207–210, doi:10.1029/91GL02940.
Labitzke, K., and H. Van Loon (1988), Associations between the 11-year solar cycle, the QBO and the atmosphere. Part I: The troposphere and stratosphere in the Northern Hemisphere in winter, *J. Atmos. Terr. Phys.*, *50*(3), 197–206.
Manzini, E., M. A. Giorgetta, M. Esch, L. Kornblueh, and E. Roeckner (2006), The influence of sea surface temperatures on the Northern Winter stratosphere: Ensemble simulations with the MAECHAM5 model, *J. Clim.*, *19*(16), 3863–3881, doi:10.1175/JCLI3826.1.
Marshall, A. G., A. A. Scaife, and S. Ineson (2009), Enhanced seasonal prediction of European winter warming following volcanic eruptions, *J. Clim.*, *22*(23), 6168–6180, doi:10.1175/2009JCLI3145.1.
McCormick, M. P., and R. E. Veiga (1992), SAGE II measurements of early Pinatubo aerosols, *Geophys. Res. Lett.*, *19*(2), 155–158, doi:10.1029/91GL02790.
Muthers, S., et al. (2014), Northern hemispheric winter warming pattern after tropical volcanic eruptions: Sensitivity to the ozone climatology, *J. Geophys. Res. Atmos.*, *119*, 1340–1355, doi:10.1002/2013JD020138.
Newman, P. A., J. F. Gleason, R. D. McPeters, and R. S. Stolarski (1997), Anomalously low ozone over the Arctic, *Geophys. Res. Lett.*, *24*(22), 2689–2692, doi:10.1029/97GL52831.
Newman, P. A., E. R. Nash, and J. E. Rosenfield (2001), What controls the temperature of the Arctic stratosphere during the spring? *J. Geophys. Res.*, *106*(D17), 19,999–20,010, doi:10.1029/2000JD000061.
Pascoe, C. L., L. J. Gray, S. A. Crooks, M. N. Juckes, and M. P. Baldwin (2005), The quasi-biennial oscillation: Analysis using ERA-40 data, *J. Geophys. Res.*, *110*, D08105, doi:10.1029/2004JD004941.
Perlwitz, J., and H.-F. Graf (1995), The statistical connection between tropospheric and stratospheric circulation of the Northern Hemisphere in winter, *J. Clim.*, *8*(10), 2281–2295, doi:10.1175/1520-0442(1995)008<2281:TSCBTA>2.0.CO;2.
Polvani, L. M., and D. W. Waugh (2004), Upward wave activity flux as a precursor to extreme stratospheric events and subsequent anomalous surface weather regimes, *J. Clim.*, *17*(18), 3548–3554, doi:10.1175/1520-0442(2004)017%3C3548:UWAFAA%3E2.0.CO;2.
Ramachandran, S., V. Ramaswamy, G. L. Stenchikov, and A. Robock (2000), Radiative impact of the Mount Pinatubo volcanic eruption: Lower stratospheric response, *J. Geophys. Res.*, *105*(D19), 24,409–24,429, doi:10.1029/2000JD900355.
Rampino, M. R., and S. Self (1982), Historic eruptions of Tambora (1815), Krakatau (1883), and Agung (1963), their stratospheric aerosols, and climatic impact, *Quat. Res.*, *18*, 127–143, doi:10.1016/0033-5894(82)90065-5.
Reichler, T., J. Kim, E. Manzini, and J. Kroger (2012), A stratospheric connection to Atlantic climate variability, *Nat. Geosci.*, *5*(11), 783–787, doi:10.1038/ngeo1586.
Reick, C. H., T. Raddatz, V. Brovkin, and V. Gayler (2013), Representation of natural and anthropogenic land cover change in MPI-ESM, *J. Adv. Model. Earth Syst.*, *5*(3), 459–482, doi:10.1002/jame.20022.
Robock, A. (2000), Volcanic eruptions and climate, *Rev. Geophys.*, *38*(2), 191–219, doi:10.1029/1998RG000054.
Robock, A., and J. Mao (1992), Winter warming from large volcanic eruptions, *Geophys. Res. Lett.*, *19*(24), 2405–2408, doi:10.1029/92GL02627.
Robock, A., and J. Mao (1995), The volcanic signal in surface temperature observations, *J. Clim.*, *8*(5), 1086–1103, doi:10.1175/1520-0442(1995)008%3C1086:TVSIST%3E2.0.CO;2.
Rozanov, E. V., M. E. Schlesinger, N. G. Andronova, F. Yang, S. L. Malyshev, V. A. Zubov, T. A. Egorova, and B. Li (2002), Climate/chemistry effects of the Pinatubo volcanic eruption simulated by the UIUC stratosphere/troposphere GCM with interactive photochemistry, *J. Geophys. Res.*, *107*(D21), 4594, doi:10.1029/2001JD000974.
Sato, M., J. E. Hansen, M. P. McCormick, and J. B. Pollack (1993), Stratospheric aerosol optical depths, 1850–1990, *J. Geophys. Res.*, *98*(D12), 22,987–22,994, doi:10.1029/93JD02553.
Schmidt, G. A., et al. (2011), Climate forcing reconstructions for use in PMIP simulations of the last millennium (v1.0), *Geosci. Model Dev.*, *4*(1), 33–45, doi:10.5194/gmd-4-33-2011.
Schmidt, G. A., et al. (2012), Climate forcing reconstructions for use in PMIP simulations of the last millennium (v1. 1), *Geosci. Model Dev.*, *5*, 185–191.
Schmidt, H., et al. (2013), Response of the middle atmosphere to anthropogenic and natural forcings in the CMIP5 simulations with the Max Planck Institute Earth system model, *J. Adv. Model. Earth Syst.*, *5*(1), 98–116, doi:10.1002/jame.20014.
Schnadt Poberaj, C., J. Staehelin, and D. Brunner (2011), Missing stratospheric ozone decrease at Southern Hemisphere middle latitudes after Mt. Pinatubo: A dynamical perspective, *J. Atmos. Sci.*, *68*(9), 1922–1945, doi:10.1175/JAS-D-10-05004.1.
Self, S., R. Gertisser, T. Thordarson, M. R. Rampino, and J. A. Wolff (2004), Magma volume, volatile emissions, and stratospheric aerosols from the 1815 eruption of Tambora, *Geophys. Res. Lett.*, *31*, L20608, doi:10.1029/2004GL020925.

Shepherd, T. G., and C. McLandress (2011), A robust mechanism for strengthening of the Brewer–Dobson circulation in response to climate change: Critical-layer control of subtropical wave breaking, *J. Atmos. Sci.*, *68*, 784–797, doi:10.1175/2010JAS3608.1.

Shindell, D. T., G. A. Schmidt, M. E. Mann, and G. Faluvegi (2004), Dynamic winter climate response to large tropical volcanic eruptions since 1600, *J. Geophys. Res.*, *109*, D05104, doi:10.1029/2003JD004151.

Sigl, M., et al. (2014), Insights from Antarctica on volcanic forcing during the Common Era, *Nat. Clim. Change*, *4*(8), 693–697, doi:10.1038/nclimate2293.

Solomon, S. (1999), Stratospheric ozone depletion: A review of concepts and history, *Rev. Geophys.*, *37*(3), 275–316, doi:10.1029/1999RG900008.

Stenchikov, G., A. Robock, V. Ramaswamy, M. D. Schwarzkopf, K. Hamilton, and S. Ramachandran (2002), Arctic Oscillation response to the 1991 Mount Pinatubo eruption: Effects of volcanic aerosols and ozone depletion, *J. Geophys. Res.*, *107*(D24), 4803, doi:10.1029/2002JD002090.

Stenchikov, G., K. Hamilton, A. Robock, V. Ramaswamy, and M. D. Schwarzkopf (2004), Arctic oscillation response to the 1991 Pinatubo eruption in the SKYHI general circulation model with a realistic quasi-biennial oscillation, *J. Geophys. Res.*, *109*, D03112, doi:10.1029/2003JD003699.

Stenchikov, G., K. Hamilton, R. J. Stouffer, A. Robock, V. Ramaswamy, B. Santer, and H.-F. Graf (2006), Arctic Oscillation response to volcanic eruptions in the IPCC AR4 climate models, *J. Geophys. Res.*, *111*, D07107, doi:10.1029/2005JD006286.

Stenchikov, G. L., I. Kirchner, A. Robock, H.-F. Graf, J. C. Antuña, R. G. Grainger, A. Lambert, and L. Thomason (1998), Radiative forcing from the 1991 Mount Pinatubo volcanic eruption, *J. Geophys. Res.*, *103*(D12), 13,837–13,857, doi:10.1029/98JD00693.

Stevens, B., et al. (2013), Atmospheric component of the MPI-M Earth system model: ECHAM6, *J. Adv. Model. Earth Syst.*, *5*(2), 146–172, doi:10.1002/jame.20015.

Stothers, R. B. (1984), The great Tambora eruption in 1815 and its aftermath, *Science*, *224*(4654), 1191–1198.

Tabazadeh, A., K. Drdla, M. R. Schoeberl, P. Hamill, and O. B. Toon (2002), Arctic "ozone hole" in a cold volcanic stratosphere, *Proc. Natl. Acad. Sci. U.S.A.*, *99*(5), 2609–2612, doi:10.1073/pnas.052518199.

Textor, C., H.-F. Graf, C. Timmreck, and A. Robock (2004), Emissions from volcanoes, in *Emissions of Atmospheric Trace Compounds*, vol. 18, edited by C. Granier, P. Artaxo, and C. Reeves, pp. 269–303, Springer, Netherlands.

Thomas, M. A., C. Timmreck, M. A. Giorgetta, H.-F. Graf, and G. Stenchikov (2009a), Simulation of the climate impact of Mt. Pinatubo eruption using ECHAM5—Part 1: Sensitivity to the modes of atmospheric circulation and boundary conditions, *Atmos. Chem. Phys.*, *9*(2), 757–769, doi:10.5194/acp-9-757-2009.

Thomas, M. A., M. A. Giorgetta, C. Timmreck, H.-F. Graf, and G. Stenchikov (2009b), Simulation of the climate impact of Mt. Pinatubo eruption using ECHAM5—Part 2: Sensitivity to the phase of the QBO and ENSO, *Atmos. Chem. Phys.*, *9*(9), 3001–3009, doi:10.5194/acp-9-3001-2009.

Timmreck, C., S. J. Lorenz, T. J. Crowley, S. Kinne, T. J. Raddatz, M. A. Thomas, and J. H. Jungclaus (2009), Limited temperature response to the very large AD 1258 volcanic eruption, *Geophys. Res. Lett.*, *36*, L21708, doi:10.1029/2005JD006286.

Toohey, M., K. Krüger, and C. Timmreck (2013), Volcanic sulfate deposition to Greenland and Antarctica: A modeling sensitivity study, *J. Geophys. Res. Atmos.*, *118*, 4788–4800, doi:10.1002/jgrd.50428.

Toohey, M., K. Krüger, M. Bittner, C. Timmreck, and H. Schmidt (2014), The impact of volcanic aerosol on the Northern Hemisphere stratospheric polar vortex: Mechanisms and sensitivity to forcing structure, *Atmos. Chem. Phys.*, *14*(11), 13,063–13,079, doi:10.5194/acp-14-13063-2014.

Trepte, C. R., and M. H. Hitchman (1992), Tropical stratospheric circulation deduced from satellite aerosol data, *Nature*, *355*, 626–628, doi:10.1038/355626a0.

Trepte, C. R., R. E. Veiga, and M. P. McCormick (1993), The poleward dispersal of Mount Pinatubo volcanic aerosol, *J. Geophys. Res.*, *98*, 18,563–18,573, doi:10.1029/93JD01362.

van Loon, H., and K. Labitzke (1987), The Southern Oscillation. Part V: The anomalies in the lower stratosphere of the Northern Hemisphere in winter and a comparison with the quasi-biennial oscillation, *Mon. Weather Rev.*, *115*(2), 357–369, doi:10.1175/1520-0493(1987)115%3C0357:TSOPVT%3E2.0.CO;2.

Zanchettin, D., O. Bothe, H. F. Graf, S. J. Lorenz, J. Luterbacher, C. Timmreck, and J. H. Jungclaus (2013), Background conditions influence the decadal climate response to strong volcanic eruptions, *J. Geophys. Res. Atmos.*, *118*, 4090–4106, doi:10.1002/jgrd.50229.